ARMA 24–715

New insights for stress conditions of laboratory shear tests

Shupeng Chai and Qi Zhao

Department of Civil and Environmental Engineering, The Hong Kong Polytechnic University, Hong Kong SAR, China

ABSTRACT: Numerous laboratory tests have been performed to investigate the shear behavior of rock discontinuities using various experimental setups. Stress heterogeneity on rock discontinuities can significantly influence the shear behavior, however, it has seldom been specified clearly. Instead, the macroscopic or average stress on the joints other than the local stress distribution was usually analyzed in most laboratory shear tests. In this study, numerical simulations considering a simple linear velocity weakening law are conducted on smooth rock joints in various laboratory setups to analyze the stress distribution before and during slip. The results show nonuniform normal and shear stress distribution in almost all the laboratory tests and significant local stress concentration near the edges of the shear surface. The estimated sample-average friction coefficient is slightly higher than the dynamic friction coefficient but lower than the static friction coefficient. Furthermore, a sudden release of the shear stress, especially near the stress-concentrated edges, can be observed in the slip phase during a stick-slip cycle. This study provides a critical review of laboratory shear tests on rock joints and contributes to our understanding of stress distribution and variation during stick-slip shear.

1. INTRODUCTION

Rock discontinuities including joints, fractures, faults, and bedding planes commonly exist in rock masses (Elsworth et al. 2016; Marone 1998). Shear failure on rock discontinuities can occur in various engineering cases, such as underground excavations including tunneling, carven and mining (Chai et al. 2023; Wu et al. 2023), slopes and dams (Chai 2023), fluid-injection projects including oil and gas extraction (Elsworth et al. 2016), enhanced geothermal systems (Zhao et al. 2020), and CO_2 or waste storage (Elsworth et al. 2016), etc. The shearing of rock discontinuities has also been reported to affect earthquake nucleation (Kaproth & Marone 2013).

Various laboratory shear setups have been developed to investigate the shear behavior of rock discontinuities. They include direct shear (DS) tests (Petit 1988), true triaxial direct shear tests (Zhao et al. 2023), single direct shear tests (Rubinstein et al. 2004), double direct shear tests (Marone 1998), triaxial direct shear tests (Frash et al. 2016), triaxial shear (TS) tests (Thompson et al. 2005), biaxial shear tests (Buijze et al. 2020), axial shear tests (Rubino et al. 2022), oblique shear tests (Ghazvinian et al. 2013), and rotary shear (RS) tests (Zhao et al. 2018). Among these test setups, the DS, TS, and RS tests are commonly used by the rock mechanics community.

In most previous laboratory tests, the average values of the normal stress (σ) and shear stress (τ) on the joint surface were used during shearing (Bedford et al. 2022; Zhao et al. 2018). However, nonuniform shear stress distribution on the shear plane generally existed in those laboratory shear setups. It may result from the difference in contacting geometries or materials (Xu et al. 2019), micro curvature of joints (Selvadurai & Glaser 2016), and dynamic stick-slip events (Ben-David et al. 2010). In particular, the sudden decrease in shear stress during repeating stick-slip shear was widely acknowledged as a laboratory phenomenon for natural earthquake initiation (Brace & Byerlee 1966). In turn, stress heterogeneity on the rock discontinuities influences earthquake nucleation (Buijze et al. 2020; Thompson et al. 2005). For instance, laboratory experiments observed a rapid declination in the shear stress near the rupture tip (Gori et al. 2021). Supershear slip was reported to be the result of increasing the local ratio of shear to normal stress (Rubinstein et al. 2004).

Thus, it is crucial to understand the influence of stress heterogeneity on the shear behavior of rock discontinuities. Some attempts have been made to measure the stress distribution in laboratory shear tests but there are some limitations. By placing an array of strain gauges along the joint, the dynamic variation of normal and shear stress distribution during shear was roughly estimated (Buijze et al. 2020), but the discretely distributed gauges may overlook local stress concentration. Digital image correlation (DIC) methods using images taken by high-speed camera could capture the full-field normal and shear stresses along the joint (Rubino et al. 2022), but the two-dimensional (2D) spatial stress distribution on the joint surface was unavailable.

Zhuo et al. (2020) employed pressure sensitive films for the normal stress distribution on the joint surface but failed to capture the dynamic evolution of stresses during shear. In contrast, numerical simulations seem to be an effective tool to capture the spatial stress distribution on rock discontinuities (Bai & Konietzky 2023; Chai 2020), whereas none has elaborately investigated the effects of stress heterogeneity on the shear behavior in the various laboratory shear setups.

In this paper, we performed a series of numerical simulations on rock joints in laboratory shear setups to capture average stress variation and overall stress distribution during shear. The effects of stress heterogeneity on shear behavior including stick-slip, friction weakening, and earthquake nucleation were discussed.

2. NUMERICAL SIMULATIONS

The numerical software, FLAC3D, was employed in this study to investigate the stress distribution on smooth rock joints in laboratory shear setups. It is based on the finite difference method and has been widely utilized in fields such as geotechnical engineering and mining engineering (Bai & Konietzky 2023; Chai 2023).

The same material properties (Table 1) were used in all the numerical models conducted for the three types of shear tests. The rock samples were considered elastoplastic, obeying the Mohr-Coulomb criteria, while steel frames were elastic.

Table 1. Material properties used in numerical simulations (taken empirically or from Frash et al. (2016)).

Parameter	Rock	Steel frame
Elastic modulus E (GPa)	12	193
Poisson's ratio υ	0.25	0.3
Density ρ (kg/m^3)	2600	8000
Internal friction angle φ (°)	40	–
Cohesion c (MPa)	20	–
Tensile strength (MPa)	2	–

Interface elements are considered for the discontinuities or weak surfaces in FLAC3D (Bai & Konietzky 2023; Chai 2023), which were applied for the rock joints here. The normal and shear stiffness of the interface elements were set to ten times the equivalent stiffness of the stiffest surrounding rocks. Zero cohesion was considered for all rock joints. A simplified linear velocity weakening law (Fig. 1) was applied in the numerical models. Empirical static (μ_s) and dynamic (μ_d) friction coefficients of rock joint were selected at 0.577 and 0.364, respectively, equivalent to friction angles of 30° and 20°. The critical velocity (v_c) when the friction weakened to μ_d was equal to the applied velocity v. The applied velocity was 1 μm/s for DS and TS tests, and an angular velocity of 0.5°/s was chosen for RS tests. For simplicity, contact surfaces existing between the rock samples and steel frames were considered smooth with zero friction and cohesion.

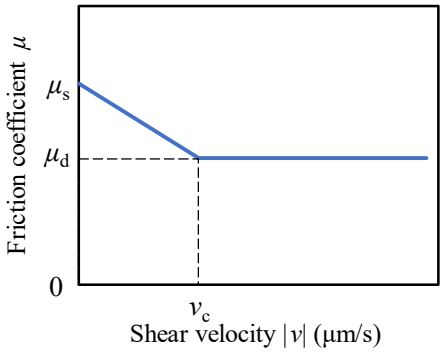

Fig. 1. Simplified linear velocity weakening law used in numerical simulations.

Numerical methods can export the normal and shear stress distributions on the interface elements directly to calculate the average normal (σ_{NJ}) and shear (τ_{NJ}) stress on the rock joints during shear. Besides, the forces required in laboratory experiments were also extracted to calculate the normal (σ_E) and shear (τ_E) stress, noted as experimental methods. Stresses and friction coefficients obtained by those two methods were compared together for each shear test to discuss the applicability of experimental methods. Three critical cases, namely, before shear (Case A), stick phase (Case B), and slip phase (Case C) in a stick-slip cycle were chosen for each laboratory test to investigate the distributions of friction angles (φ_J), normal (σ) and shear stress (τ) on the joint surface.

3. RESULTS

3.1. Direct shear (DS) tests

In the numerical model for DS tests (Fig. 2a), the sample dimensions for the two separate rock blocks are 150 mm × 150 mm × 75 mm. Fig. 2b indicates a constant average normal stress of 5 MPa, equal to the applied normal stress (σ_N). The variation of average stresses and friction coefficients obtained from laboratory and numerical methods demonstrated good consistency and obvious stick-slip shear behavior. The average friction coefficient of the rock joint was about 0.382, slightly larger than μ_d (0.364). A slight rotation around the shear edge in DS tests can be observed (Fig. 2c) and significant stress concentration occurred near the rotating edge.

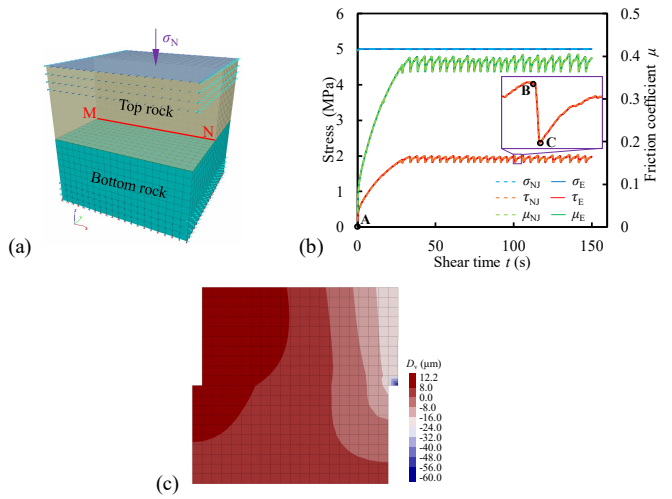

Fig. 2. Numerical modeling of direct shear tests: (a) A typical numerical model. Line MN is used for position identification of the interface elements. (b) Variations of average shear and normal stress on the interface and friction coefficient of the interface with shear time t. The shear time for Cases DS-A, B, and C is also marked. (c) Vertical displacement contour at a shear displacement of 0.5 mm.

To analyze the stress variation on the joint surface, the spatial distributions of σ, τ, and φ_J on the joint interface were visualized in Fig. 3. Before shear (Case DS-A), σ distributed uniformly at 5 MPa (Fig. 3a) and no shear occurred (Figs. 3b and c). Nonuniform distribution of σ and τ existed throughout the shear stage in DS tests and stresses concentrated near the right edge of the shear surface (Figs. 3d, e, g, and h). During the transition from stick phase (Case DS-B) to slip phase (Case DS-C) of the stick-slip cycle shown in Fig. 2b, the maximum σ decreased from 12.46 (Fig. 3d) to 11.79 MPa (Fig. 3g). In comparison, τ decreased from 6.25 (Fig. 3e) to 4.29 MPa (Fig. 3h). Near the right edge of the joint surface, most of the interface elements changed from a static state (φ_J = 30°, Fig. 3f) to a dynamic state (φ_J = 20°, Fig. 3i). In Case DS-B, the average normal and shear stresses on the joint were about 5.01 MPa and 1.99 MPa, respectively, resulting in an average friction angle of about 21.63°. In contrast, the average friction angle in Case DS-C was 20.03°.

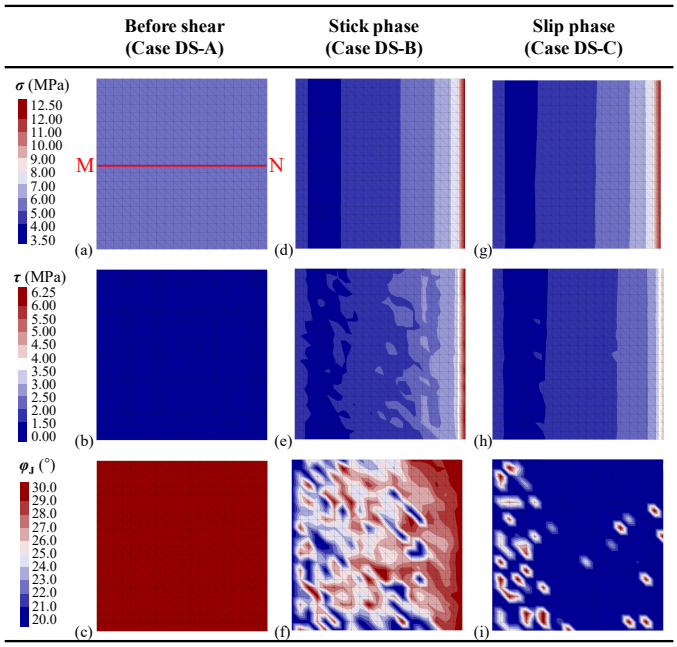

Fig. 3. Distributions of normal and shear stresses and friction angles on the joint interface in direct shear tests for Cases DS-A (a, b, c), DS-B (d, e, f), and DS-C (g, h, i).

3.2. *Triaxial shear (TS) tests*

Fig. 4a shows the numerical model for the TS test. The diameter and height of the complete sample are 50 and 100 mm, respectively. An inclined joint passing the model center with an inclination angle of 30° to the axial direction formed later. The confining pressure around the sample was 10 MPa. Fig. 4b suggested that average stresses and friction obtained by the two methods achieve good accordance. The average normal and shear stress increased continuously during shearing until reaching a stick-slip shear. The variation of average normal stress dependent on the applied maximum principal stress differed from the constant conditions in direct shear tests. Based on the experimental curve for μ_E, the average friction coefficient was about 0.388, which was also higher than μ_d (0.364).

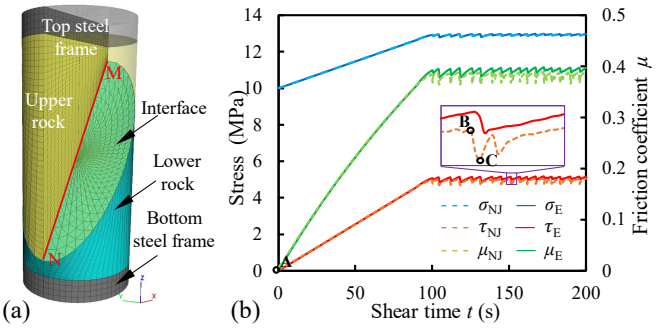

Fig. 4. Numerical modeling of triaxial shear tests: (a) A typical numerical model. (b) Variations of average shear and normal stress on the right interface and friction coefficient of the interface with shear time t. The shear time for Cases TS-A, B, and C is also marked.

Fig. 5 shows the stress and friction contours on the joint surface in the TS test for Cases TS-A, B, and C (Fig. 4b). In Case TS-A, no shear slip occurred (Fig. 5c), σ distributed uniformly at 10 MPa (Fig. 5a) and τ remained around zero (Fig. 5b) on the joint surface. However, slight normal stress heterogeneity emerged in the stick phase (Case TS-B) and slip phase (Case TS-C). The maximum and average normal stress on the joint surface were 13.42 (Fig. 5d) and 12.95 MPa in Case TS-B, while were 13.40 (Fig. 5g) and 12.95 MPa in Case TS-C. Nevertheless, τ and φ_J in the stick phase showed remarkable heterogeneity, with a maximum τ of 6.24 MPa (Fig. 5e) and an average shear stress of 5.00 MPa. In the following slip phase, the shear stress near the bottom dropped suddenly, and the maximum and average shear stress decreased to 5.63 (Fig. 5h) and 4.79 MPa, respectively. Besides, a sliding trend could also be inferred by the dynamic friction angle (φ_J = 20°, Fig. 5i) declined from 30° (φ_s, Fig. 5f).

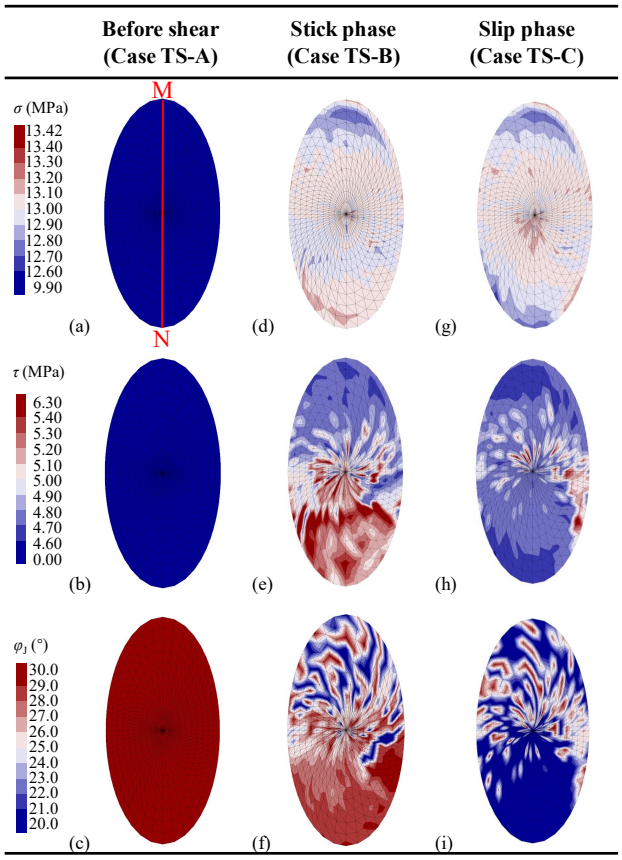

Fig. 5. Distributions of normal and shear stresses and friction angles on the joint interface in triaxial shear tests for Cases TS-A (a, b, c), TS-B (d, e, f), and TS-C (g, h, i).

3.3. Rotary shear (RS) tests

The numerical model for the rotary shear tests under normal stress of 5 MPa was presented in Fig. 6a. The angular rotation at 0.5°/s was applied at the top two-fifths of the upper block, which was confined by a steel frame. The average stresses and friction coefficient on the rock joint were estimated only by numerical methods (Fig. 6b). The average normal stress remained constant throughout the shearing process while the average shear stress showcased stick-slip behavior. The average friction coefficient of the rock joint was estimated at 0.374 and surpassed μ_d (0.364).

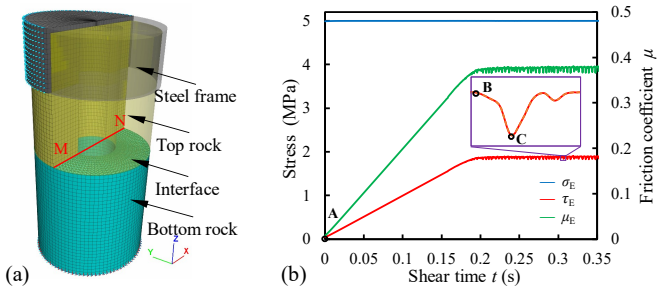

Fig. 6. Numerical modeling of rotary shear tests: (a) A typical numerical model. The model base is fixed in all directions. (b) Variations of average shear and normal stress on the right interface and friction coefficient of the interface with shear time t. The shear time for Cases RS-A, B, and C is also marked.

Fig. 7 presents the stress and friction contours on the joint surface in the RS test for Cases RS-A, B, and C (Fig. 6b). σ was almost constant at around 5 MPa before (Fig. 7a) and during (Figs. 7d and g) the shearing process with a deviation of 2.9% compared with the maximum σ. Before applying the rotary force, no slip emerged (Fig. 7c), and the shear stress was close to 0 (Fig. 7b). Shear stress heterogeneity existed during shearing (Figs. 7e and h). Compared with Case RS-B for the stick phase, the maximum shear stress dropped from 2.42 (Fig. 7e) to 2.28 MPa (Fig. 7h) in Case RS-C for the slip phase. Additionally, most interface elements change to a dynamic condition with φ_d = 20° in the slip phase.

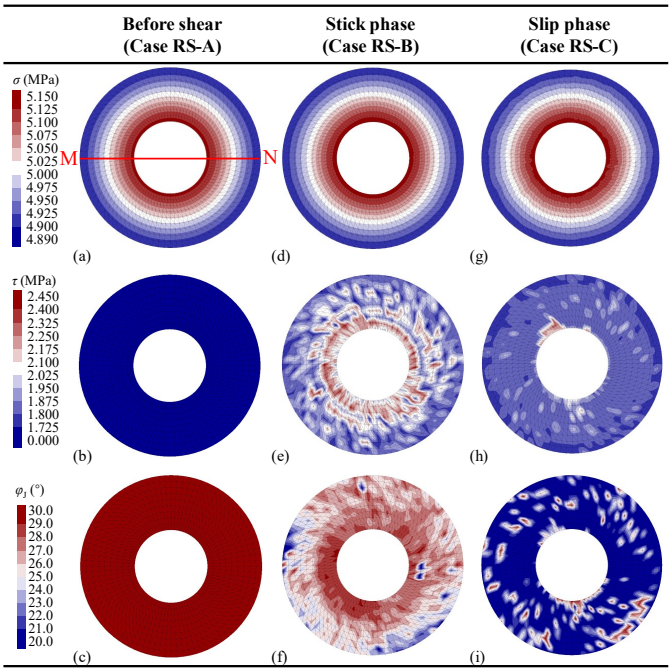

Fig. 7. Distributions of normal and shear stresses and friction angles on the right joint interface in double direct shear tests for Cases RS-A (a, b, c), RS-B (d, e, f), and RS-C (g, h, i).

4. DISCUSSION

4.1. Stick-slip behavior

Numerical results have indicated significant stress heterogeneity on smooth rock joints in all laboratory setups. In all direct and inclined shear tests, a bowl-shaped stress distribution with stress concentrations near the edge could be observed along the shear direction (line MN in each test). It agrees well with previous laboratory measurements based on strain gauges (Wu & McLaskey 2019; Xu et al. 2019).

For the comparison between different laboratory shear tests, normalized stress concentration coefficients for normal R_{Nmax} and shear R_{Smax} stress are estimated by

$$R_{\mathrm{Nmax}}=\frac{\sigma_{\max}}{\sigma_{\mathrm{avg}}} \tag{1}$$

$$R_{\mathrm{Smax}}=\frac{\tau_{\max}}{\tau_{\mathrm{avg}}} \tag{2}$$

Similarly, the ratios for the minimum normal R_{Nmin} and shear R_{Smin} stress on the rock joint are obtained by

$$R_{\mathrm{Nmin}}=\frac{\sigma_{\min}}{\sigma_{\mathrm{avg}}} \tag{3}$$

$$R_{\mathrm{Smin}}=\frac{\tau_{\min}}{\tau_{\mathrm{avg}}} \tag{4}$$

where $\sigma_{\max}$, $\sigma_{\min}$, σ_{avg} are the maximum, minimum, and average normal stress on the shear plane, respectively while $\tau_{\max}$, $\tau_{\min}$, τ_{avg} are the maximum, minimum, and average shear stress. The calculated normal and shear stress ratios for the three cases in each shear test are presented in Fig. 8.

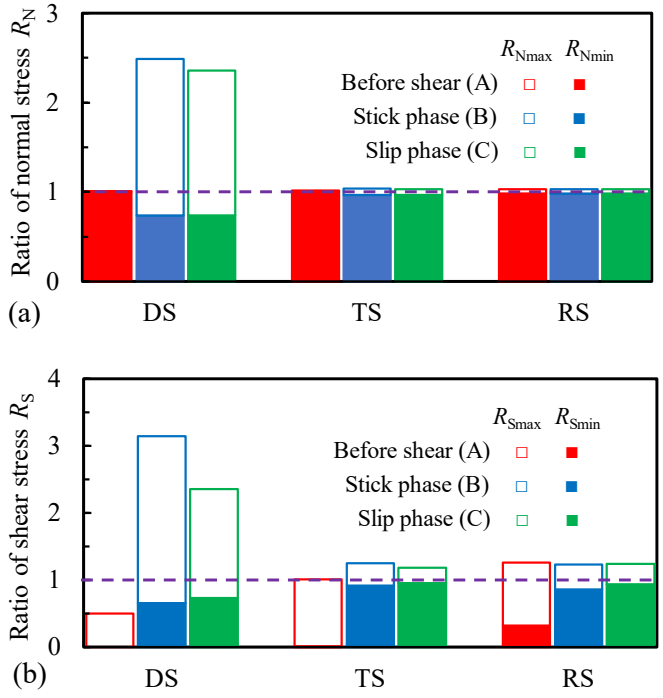

Fig. 8. Ratio of the maximum and minimum stress to the average stress in different laboratory shear tests: (a) Normal stress and (b) Shear stress.

Before shearing, σ distributed almost uniformly on the joints in DS, TS, and RS tests. Once shearing starts, significant stress heterogeneity occurred in the DS test for both normal and shear stress. This is because the rotating trend of the sliding rock (Petit 1988) caused high stress concentration near the rotation edge (Fig. 2b). The normal stress distribution in TS and RS can be regarded as uniform while shear stress heterogeneity cannot be ignored.

When changing from the stick phase to the slip phase, the stress distribution on the rock joint becomes less uniform with smaller stress ratios. It can be attributed to the release of strain energy accumulated in the previous stick stage, causing a decrease in stress, especially near highly stress-concentrated edges. During stick-slip shear, such long-term cycles of stress concentrations and releases may induce dynamic damage to the smooth rock joints, especially near the edges.

4.2. Friction weakening

In numerical simulations, a simplified linear velocity weakening friction law was applied to every gridpoint (Fig. 1), and the local friction coefficient changed accordingly after each calculation step. The configuration differed from most previous laboratory tests, in which the friction weakening behavior was analyzed based on the loading velocity (Marone 1998) or average velocity on the joints (Han et al. 2010). If the loading velocity is used as a criterion in this study, the numerical cases with a constant loading velocity throughout the shearing procedure will theoretically not experience any velocity-dependent weakening. The considered numerical configuration can overcome the limitations. In the slip phase, cumulative strain energy is released rapidly, especially near highly stress-concentrated areas (Bedford et al. 2022), causing an increase in local sliding velocity and local friction weakening. Later, friction heals with declining local sliding velocity, thus resulting in energy accumulation and stress concentration (Marone 1998). It is worth noting that slip weakening friction law was not incorporated into the numerical simulations, but slip weakening and healing behavior appeared, as shown in Fig. 9.

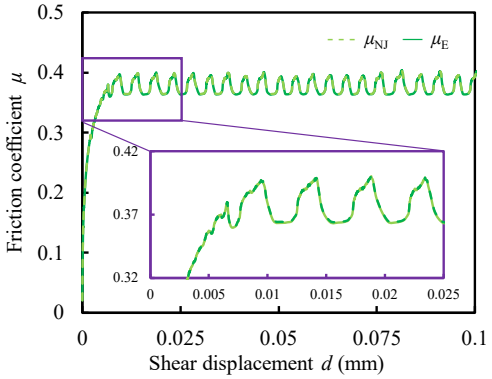

Fig. 9. Slip weakening and healing in DS tests.

4.3. *Earthquake nucleation*

Considering the simple linear velocity weakening model (Fig. 1) used in the numerical simulations, the friction angle can reflect the shear velocity at each gridpoint and can be applied for earthquake nucleation analyses. Different from previous laboratory or numerical measurements with limited velocity data on only one or two lateral sides (Xu et al. 2019), the two-dimensional distribution of joint parameters including shear stress and friction angle during rupture initiation and propagation can be captured. Fig. 10 shows an example of the DS test.

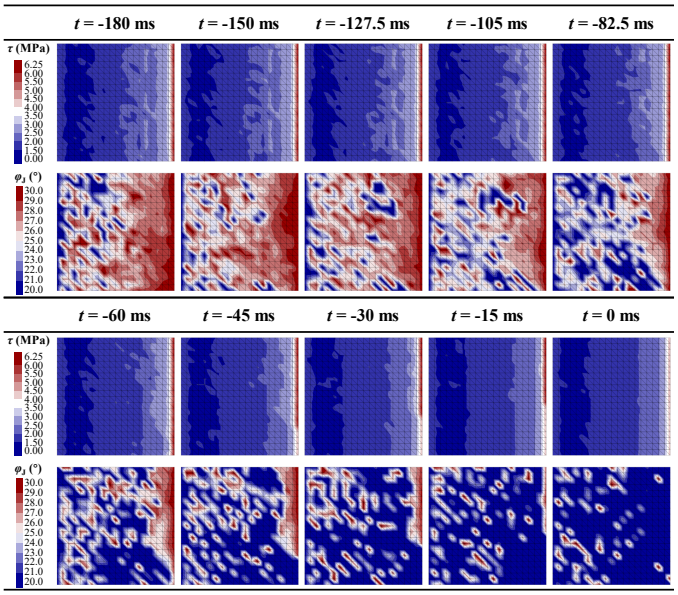

Fig. 10. Shear stress and friction angle distribution on the joint surface during rupture initiation and propagation in DS tests. t is the relative time, and $t = 0$ is when a complete joint rupture occurs.

In the DS tests, the rupture initiated near the bottom of the shear loading side, then propagated upwards, and finally reached the right edge. Due to the limited joint dimension, a complete rupture formed in this case (Wu & McLaskey 2019). Similar to previous laboratory observations (Rubino et al. 2022), the shear stress dropped significantly as the rupture front swiped through, especially near the edges starting from 60 ms before the complete rupture. Such rupture nucleation analyses have been conducted for all the numerical simulations shown in Section 3, and sound consistency between shear stress drop and rupture tip propagation could be obtained.

5. CONCLUSION

Nonuniform stress distribution on rock discontinuities has been widely reported in numerous laboratory shear tests and can significantly influence shear behavior. However, the effect of stress heterogeneity has not been specified in most laboratory shear tests. In this paper, a series of numerical simulations were conducted to investigate the stress distributions in shear tests quantitatively. The interior mechanisms between stress heterogeneity and the shear behavior were then discussed. Some main findings are summarized as follows.

(i) Numerical simulations for laboratory shear tests demonstrated nonuniform normal and shear stress distribution on the rock joints. The stresses are concentrated near the edge of rock samples during shear. More pronounced stress heterogeneity could be observed in the DS test.

(ii) The estimated average friction coefficient during stick-slip shear was slightly higher than the dynamic friction coefficient but lower than the static friction coefficient.

(iii) The local shear stress dropped significantly when the rupture tip swiped through or in the following slip phase during a stick-slip cycle, causing the stress distribution to become less nonuniform.

REFERENCES

1. Bai, Q., & Konietzky, H. (2023). A weakening-healing law to simulate stick-slip behavior of rock joint and the associated seismicity. *IOP Conf. Ser. Earth Environ. Sci., 1124*(1), 012059. doi:10.1088/1755-1315/1124/1/012059.
2. Bedford, J. D., Faulkner, D. R., & Lapusta, N. (2022). Fault rock heterogeneity can produce fault weakness and reduce fault stability. *Nat. Commun., 13*(1), 326. doi:10.1038/s41467-022-27998-2.
3. Ben-David, O., Cohen, G., & Fineberg, J. (2010). The Dynamics of the Onset of Frictional Slip. *Science, 330*(6001), 211-214. doi:10.1126/science.1194777.
4. Brace, W. F., & Byerlee, J. D. (1966). Stick-Slip as a Mechanism for Earthquakes. *Science, 153*(3739), 990-992. doi:10.1126/science.153.3739.990.
5. Buijze, L., Guo, Y., Niemeijer, A. R., Ma, S., & Spiers, C. J. (2020). Nucleation of Stick-Slip Instability Within a Large-Scale Experimental Fault: Effects of Stress Heterogeneities Due to Loading and Gouge Layer Compaction. *J. Geophys. Res. Solid Earth, 125*(8), e2019JB018429. doi:10.1029/2019JB018429.
6. Chai, S. (2020). *Analytical and numerical studies on the stresses in backfilled stopes and the stability of side-exposed backfill in inclined stopes.* Master Thesis, Polytechnique Montreal, Montreal, QC, Canada.
7. Chai, S. (2023). Two-wedge slope stability analysis considering a nonvertical wedge interface. *B. Eng. Geol. Environ., 82*(3), 89. doi:10.1007/s10064-023-03126-2.
8. Chai, S., Zheng, J., & Li, L. (2023). Kink effect on the stress distribution in 2D backfilled stopes. *Geotech. Geol. Eng., 41*(5), 3225-3238. doi:10.1007/s10706-023-02434-4.
9. Elsworth, D., Spiers, C. J., & Niemeijer, A. R. (2016). Understanding induced seismicity. *Science, 354*(6318), 1380-1381. doi:10.1126/science.aal2584.
10. Frash, L. P., Carey, J. W., Lei, Z., Rougier, E., Ickes, T., & Viswanathan, H. S. (2016). High-stress triaxial direct-shear fracturing of Utica shale and in situ X-ray microtomography with permeability measurement. *J. Geophys. Res. Solid Earth, 121*(7), 5493-5508. doi:10.1002/2016JB012850.

11. Ghazvinian, A., Vaneghi, R. G., Hadei, M. R., & Azinfar, M. J. (2013). Shear behavior of inherently anisotropic rocks. *Int. J. Rock Mech. Min. Sci., 61* 96-110. doi:10.1016/j.ijrmms.2013.01.009.
12. Gori, M., Rubino, V., Rosakis, A. J., & Lapusta, N. (2021). Dynamic rupture initiation and propagation in a fluid-injection laboratory setup with diagnostics across multiple temporal scales. *Proceedings of the National Academy of Sciences, 118*(51), e2023433118. doi:10.1073/pnas.2023433118.
13. Han, R., Hirose, T., & Shimamoto, T. (2010). Strong velocity weakening and powder lubrication of simulated carbonate faults at seismic slip rates. *J. Geophys. Res. Solid Earth, 115*(B3). doi:10.1029/2008JB006136.
14. Kaproth, B. M., & Marone, C. (2013). Slow Earthquakes, Preseismic Velocity Changes, and the Origin of Slow Frictional Stick-Slip. *Science, 341*(6151), 1229-1232. doi:10.1126/science.1239577.
15. Marone, C. (1998). The effect of loading rate on static friction and the rate of fault healing during the earthquake cycle. *Nature, 391*(6662), 69-72. doi:10.1038/34157.
16. Petit, J. P. (1988). Normal stress dependent rupture morphology in direct shear tests on sandstone with applications to some natural fault surface features. *Int. J. Rock Mech. Min. Sci. Geomech. Abstr., 25*(6), 411-419. doi:10.1016/0148-9062(88)90981-3.
17. Rubino, V., Lapusta, N., & Rosakis, A. J. (2022). Intermittent lab earthquakes in dynamically weakening fault gouge. *Nature, 606*(7916), 922-929. doi:10.1038/s41586-022-04749-3.
18. Rubinstein, S. M., Cohen, G., & Fineberg, J. (2004). Detachment fronts and the onset of dynamic friction. *Nature, 430*(7003), 1005-1009. doi:10.1038/nature02830.
19. Selvadurai, P. A., & Glaser, S. D. (2016). Asperity generation and its relationship to seismicity on a planar fault: a laboratory simulation. *Geophys. J. Int., 208*(2), 1009-1025. doi:10.1093/gji/ggw439.
20. Thompson, B. D., Young, R. P., & Lockner, D. A. (2005). Observations of premonitory acoustic emission and slip nucleation during a stick slip experiment in smooth faulted Westerly granite. *Geophys. Res. Lett., 32*(10). doi:10.1029/2005GL022750.
21. Wu, B. S., & McLaskey, G. C. (2019). Contained Laboratory Earthquakes Ranging From Slow to Fast. *J. Geophys. Res. Solid Earth, 124*(10), 10270-10291. doi:10.1029/2019JB017865.
22. Wu, H., Zhao, Q., Shen, J., & Li, H. (2023). *Numerical Simulation of the Underground Storage Cavern Using FDEM.* Paper presented at the 57th U.S. Rock Mechanics/Geomechanics Symposium. doi:10.56952/arma-2023-0282.
23. Xu, S., Fukuyama, E., & Yamashita, F. (2019). Robust Estimation of Rupture Properties at Propagating Front of Laboratory Earthquakes. *J. Geophys. Res. Solid Earth, 124*(1), 766-787. doi:10.1029/2018JB016797.
24. Zhao, J., Hu, L., Feng, X., Xiao, Y., & Guo, Y. (2023). Shear Failure Mechanisms of Sandstone Subjected to Direct, True Triaxial and Confining Shear Test Conditions. *Rock Mech. Rock Eng., 56*(9), 6889-6903. doi:10.1007/s00603-023-03410-3.
25. Zhao, Q., Glaser, S. D., Lisjak, A., & Grasselli, G. (2020). *Numerical Simulation of Fault Slip During Geothermal Energy Extraction.* Paper presented at the 54th U.S. Rock Mechanics/Geomechanics Symposium.
26. Zhao, Q., Tisato, N., Kovaleva, O., & Grasselli, G. (2018). Direct Observation of Faulting by Means of Rotary Shear Tests Under X-Ray Micro-Computed Tomography. *J. Geophys. Res. Solid Earth, 123*(9), 7389-7403. doi:10.1029/2017JB015394.
27. Zhuo, Y., Guo, Y., Chen, S., & Ji, Y. (2020). Laboratory study on the effects of fault waviness on granodiorite stick-slip instabilities. *Geophys. J. Int., 221*(2), 1281-1291. doi:10.1093/gji/ggaa088.